JOURNAL OF MATERIALS SCIENCE 30 (1995) 426–436

Heat capacities of aluminium alloys*

A.-M. ZAHRA, C. Y. ZAHRA
Centre de Thermodynamique et de Microcalorimétrie, C.N.R.S. 26, rue du 141ème R.I.A., F-13003 Marseille, France

G. JAROMA-WEILAND, G. NEUER
IKE, Universität Stuttgart, Pfaffenwaldring 31, D-7000 Stuttgart 80, Germany

W. LACOM
Österreichisches Forschungszentrum Seibersdorf, A-2444 Seibersdorf, Austria

In the framework of the European COST 507 project the specific heat capacities of aluminium alloys and metal matrix composites based thereon have been measured between 20 and 520 °C by differential scanning calorimetry and stored in the databank THERSYST along with other thermophysical properties mainly drawn from literature. The curves show the influence of additional elements and reinforcements, of the fabrication process, thermomechanical treatment and scanning rate on the precipitation and dissolution kinetics of the various metastable phases and their relative amounts. The database may be used to select existing light alloys or elaborate new ones in view of specific technical applications.

1. Introduction

Aluminium based alloys find wide technical applications owing to the presence of metastable phases which improve their performance and service properties. They are used in aerospace and marine engineering, for transport, structural and sport equipments. The mechanical, physical and chemical properties of the various alloys depend on their phase constitution whose knowledge is fundamental to industrial application and future development.

The metastable phases remain coherent with the matrix as long as their sizes are small and introduce coherency strains as well as long-range elastic stresses. As the energy of the alloy system depends on volume fraction, size, shape and distribution of these phases, the usual thermodynamic equilibrium conditions or extrapolations therefrom no longer apply and experimental work becomes indispensable.

Different combinations of alloy composition and heat treatment lead to different metallurgical states whose stabilities are reflected in the heat capacity evolution with temperature. Positive deviations from linear variation according to the Neumann–Kopp rule indicate dissolution and negative deviations precipitation processes occurring during the heating.

It would be too time consuming to establish the c_p-curves for all alloys of industrial interest. Hence it is one of the aims of a European research programme to characterize each family in order to check the validity of heat treatments, to identify the microstructures present and to predict the behaviour of similar alloys. Within the COST action 507 started in 1990, c_p-measurements are performed on binary, ternary and quaternary as well as on technical aluminium alloys, and the resulting curves are commented upon and stored in the databank THERSYST [1] along with c_p-values already published in literature. As this databank is much more general and covers values of many other thermophysical properties, like thermal and electrical conductivities, thermal expansion and diffusivity, it may guide users to select or elaborate new light alloys in view of specific technical applications.

2. Experimental

As aluminium alloys are characterized by the occurrence of non equilibrium phases with more or less slow diffusion kinetics, dynamic heat capacity measurements are carried out. A Perkin-Elmer DSC-2 instrument is employed at a heating rate of 10 K min^{-1} and a DuPont thermal analyser, model 990, is used up to 520 (400) °C at 20 K min^{-1}. This last rate is the highest acceptable without having to correct for thermal inertia, and favours structural evolution during the scan much less than slower rates. The calibration of the apparatus is performed with the help of a sapphire reference sample. The alloys are in the form of discs 6 mm in diameter and 1 mm thick, their masses are about 70 mg. Heat capacity values are determined by the scanning method [2] from three runs in air; three specimens are examined in general. The reproducibility of the c_p-data is $\pm$ 2%.

The chemical compositions of the materials selected for this paper are given with the results in mass %; they comprise Al–Cu, Al–Zn, Al–Si, Al–Mg–Si, Al–Cu–Mg, Al–Zn–Mg as well as industrial alloys of the series 2xxx, 5xxx, 6xxx and 7xxx supplied by Austria Metall AG. The influence of alloy composition

* Dedicated to Professor Dr. Hans Löffler on the occasion of his 72nd birthday.

0022–2461

and different heat treatment parameters on the c_p-evolution is studied; in the case of technical wrought alloys, the type of material processing and the final sheet thickness after warm and cold rolling are varied as well. All these specifications enter the databank. Whenever possible, the c_p-curves obtained are compared with literature values also stored in the databank. These values have been assessed by means of dynamic c_p-measurements using differential scanning calorimetry (DSC) apparatuses, like in reference [3], or Nagasi–Takagi type instruments, as in reference [4]. The latter enable only studies at low heating rates.

The database THERSYST [1] is a combination of a factual database for thermophysical properties of solid materials with a modular program system to handle the database content. As the thermophysical properties depend on material parameters and experimental conditions (meta-data), the information on all factors of influence is stored and the original context between a set of experimental data and the meta-data is preserved. The physical information is converted into a standardized form given by the THERSYST scheme of category, which is divided into five hierarchically structured classes: material designation, material characterization, experiment description, thermophysical property data and bibliography. The THERSYST modular program system enables data selection corresponding to the criteria defined by users, data manipulation (e.g. conversion of units, variable transformation, regression of data) and representation of data in form of tables and graphs.

Altogether 1193 data sets on 126 different light metal alloys and MMCs have been stored up to now. About 250 new data were obtained during the COST 507 action, the others were taken from literature.

3. Results and discussion

3.1. Al–Cu alloys

The c_p-curves presented in Figs 1 and 2 refer to different sets of chemical composition, heat treatment and scan rate, as given in the figure captions.

When solid solutions of copper in aluminium are aged at room temperature (RT or 20 °C), metastable Guinier–Preston (GP) zones are formed. They become unstable upon heating, as indicated by a stronger increase in the c_p-values above 100 °C (Fig. 1). Some GP zones may still grow during the scan and get dissolved at somewhat higher temperatures owing to more stable configurations. The precipitation of metastable θ′ sets in above 250 °C; it starts the earlier and is the more important, the lower the scan rate. θ′-dissolution with concomitant occurrence of the stable θ-phase is followed by θ-dissolution before the attainment of the high temperature solid solution [6].

If ageing is carried out at 160 °C, the corresponding c_p-curve (Fig. 2) infers the presence of the θ″-phase from reversion temperatures intermediate between those for GP zones and θ′. At 130 °C, both GP zones and θ″ are formed. The θ″-phase never appears as first phase but develops from GP zones either isothermally or at heating rates below 10 K min^{-1} [8].

3.2. Al–Zn alloys

Fig. 3 illustrates the influence of alloy composition in case of binary Al alloys containing 6–37% Zn; with increasing zinc concentration, the c_p-values decrease. For comparison, the values for pure Al are also shown [9]. After solutionizing at 400 °C, water quenching

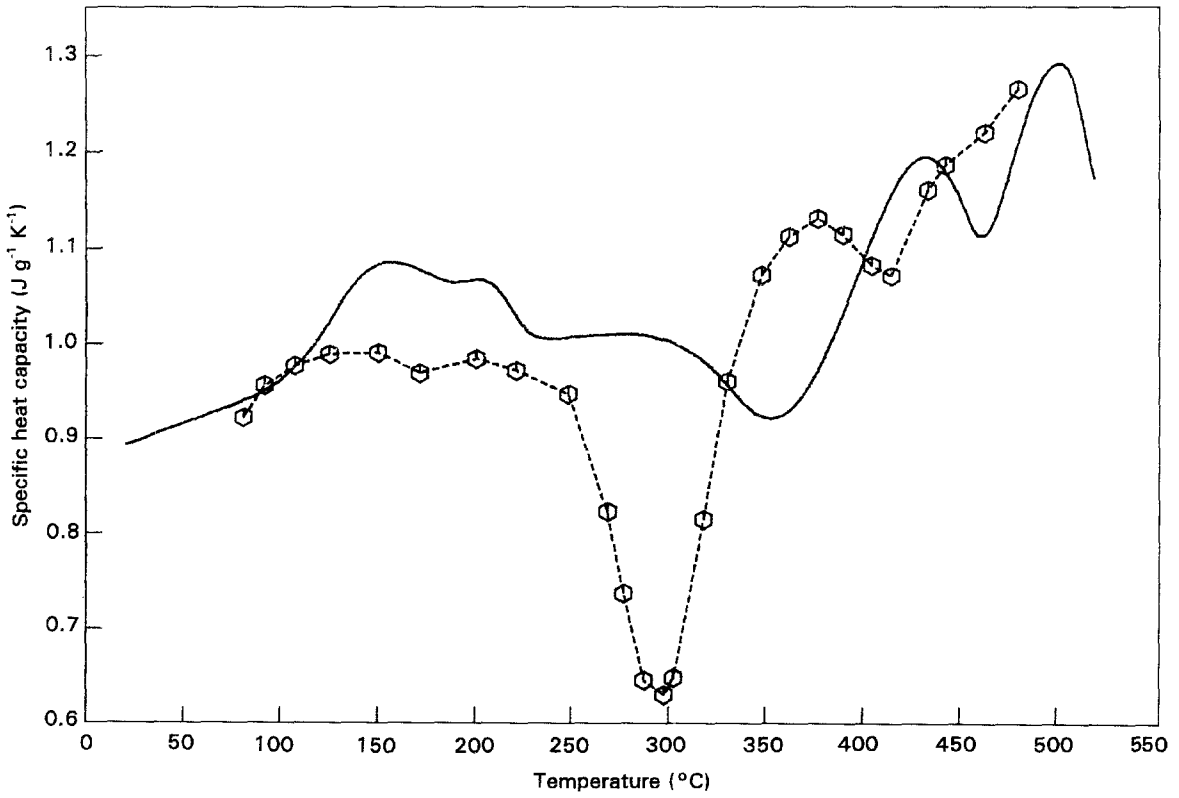

Figure 1 c_p-Evolution of binary Al–Cu alloys. – ⬡ – –, E0007038 [5] Al–4.8% Cu 50 h 525 °C → cold water → 32 d/RT ≅ 2 K min^{-1}; ——, E8000075 Al-4% Cu 2 h 525 °C → 0 °C → 84 d/RT 20 K min^{-1}.

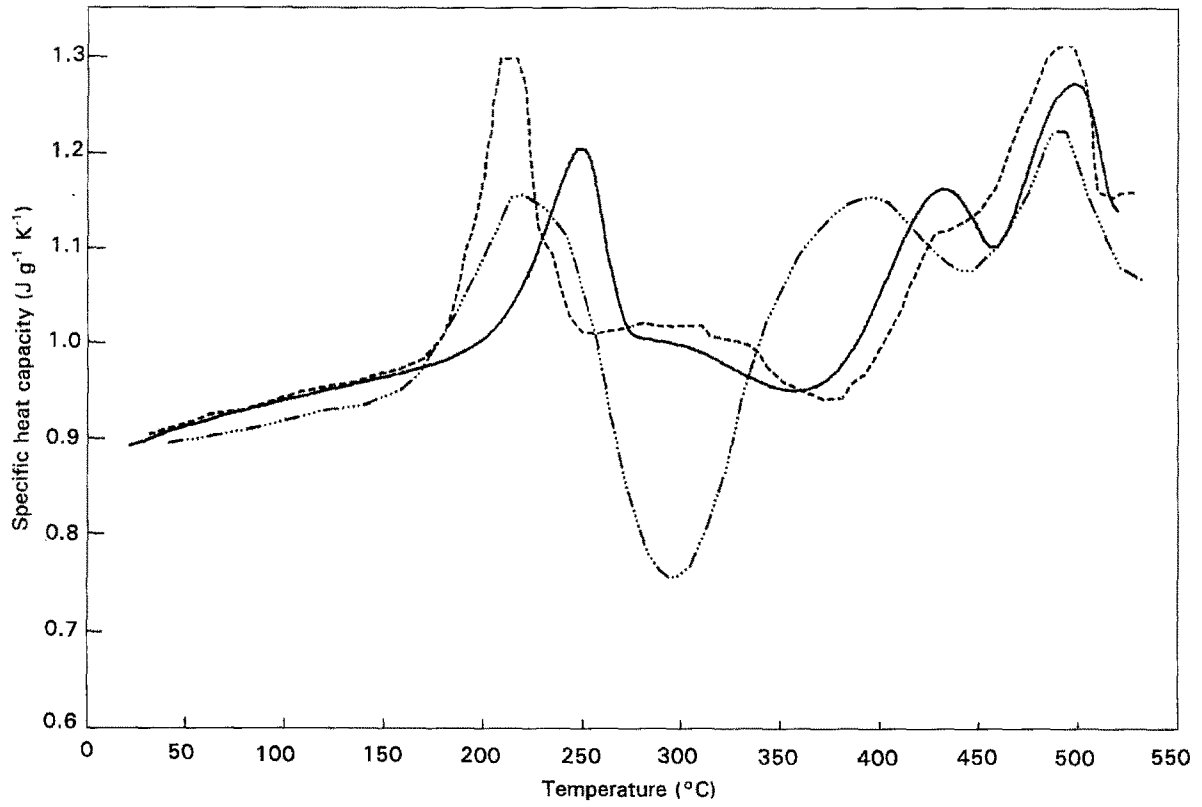

Figure 2 c_p-Evolution of binary Al–Cu alloys. – – –, E0007051 [7] Al-3.9% Cu 1 h 540 °C → 0 °C → 120 h/130 °C 10 K min^{-1}; – · · · –, E0007171 [4] Al-4% Cu 24 h/540 °C → 18 °C → 136 h/130 °C 2–3 K min^{-1}; ——, E8000072 Al-4% Cu 2 h 525 °C → 0 °C → 48 h/160 °C 20 K min^{-1}.

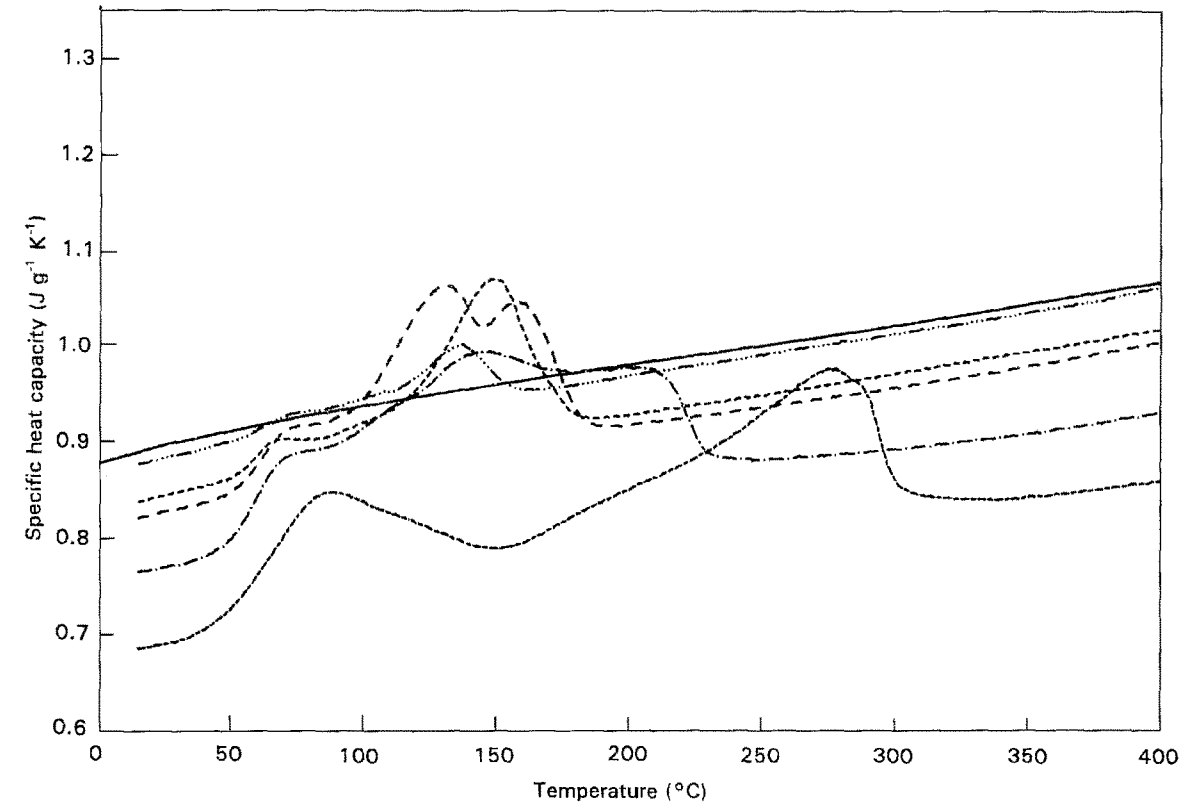

Figure 3 c_p-Evolution of pure Al and of binary Al–Zn alloys heat treated (2 h/400 °C → 0 °C → 24 h/RT); scanning rate 20 K min^{-1}. ——, E0006638 [9] Al; —· · ·, E8000100 Al-5.84% Zn; – – –, E8000103 Al-10.1% Zn; – – –, E8000108 Al-15.0% Zn; – · – ·, E8000110 Al-25.04% Zn; – – – -, E8000111 Al-36.7% Zn.

and ageing for a day at 20 °C, GP zones of spherical and ellipsoidal forms are present. Their reversion during the DSC analysis at 20 K min^{-1} causes the first two peaks situated below and above 100 °C. The third event around 160 °C gives indirect evidence for the presence of the α'_R-phase, i.e. large sized GP zones [10]. They exist already at RT, as GP zone growth during heating at 20 K min^{-1} is not important [11].

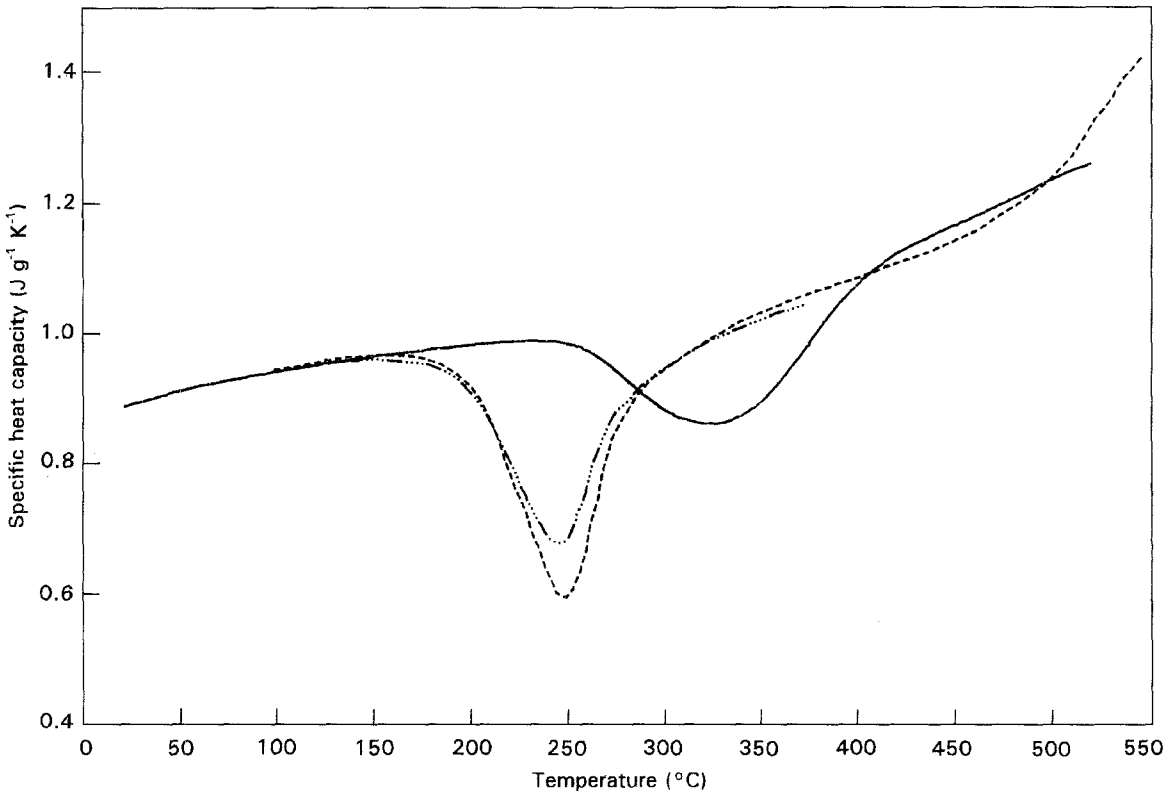

Figure 4 c_p-Evolution, at 20 K min^{-1}, of binary Al–Si solid solutions. – – –, E0007207 [14] Al-2.4% Si melt spun 5 min/550 °C → 0 °C; —·—, E0007208 [14] Al-1.3% Si melt spun 5 min/550 °C → 0 °C; ——, E8000184 Al-5.8% Si 2 h/550 °C → 0 °C.

As to the Al-25% Zn alloy, the metastable α'_m-phase dissolves around 200 °C.

In zinc rich compositions, discontinuous precipitation of nearly pure zinc occurs besides the continuous precipitation mechanism. The c_p-curve for an Al-37% Zn alloy shows GP zone reversion and Zn-dissolution which ends up in the monotectoid reaction [12].

3.3. Al-Si alloys

These alloys constitute an exception as the equilibrium phase, pure Si, precipitates directly from the matrix. The maximum solubility of Si in Al is 1.3% at 550 °C and < 0.01% at RT [13].

The influence of quenching rate from the same solutionizing temperature on silicon precipitation during the scan is illustrated in Fig. 4. In the case of melt-spun ribbons quenched into ice water, the equilibrium phase appears much earlier than in the case of cast, massive samples, presumably owing to a higher concentration of quenched-in excess vacancies which condense to dislocation loops and facilitate the nucleation of silicon atom clusters around 200 °C [15]. RT ageing also enhances silicon precipitation at higher temperatures.

3.4. Ternary Al–Mg–Si alloys

Fig. 5 shows the influence of heating rate on the c_p-evolution of water-quenched alloys; the respective chemical composition, heat treatment and scan rate are given in the caption. Heating starts out with GP zone formation, which is much better visualized at 20 K min^{-1} than at rates ten times lower; after their partial dissolution, ordered GP zones (β″-phase) appear, closely followed by the still metastable β′-phase. At a rate of 2 K min^{-1}, precipitation of the equilibrium phase β (Mg_2Si) is seen to occur around 400 °C; its redissolution is accomplished before 600 °C. After RT ageing, a more intensive formation of the β″-phase is seen to occur.

3.5. Ternary Al–Cu–Mg alloys

c_p-Measurements on quenched ternary solid solutions differing mainly in magnesium content are given in Fig. 6. The amounts of metastable and stable phases precipitated are greater in the alloy containing more magnesium, because there are more such atoms and their strong affinities to vacancies and copper atoms ensure easy diffusion even at a ten times higher scan rate. The formation of GPB zones provokes the first c_p-decrease; the exothermal effect superimposed on GPB zone reversion may be attributed to the formation of the metastable S″-phase [19]. S′ and S (Al_2CuMg) precipitations lead to falling c_ps before final dissolution. This figure also confirms that RT ageing after quenching enhances the formation rate of the S′-phase which may nucleate on dislocation loops and helices produced by the condensation of vacancies during prolonged ageing [20]. GPB zones are more stable than GP zones in binary Al–Cu alloys (Fig. 1) as indicated by their reversion temperatures. The respective enthalpy values show that during heating, much more precipitation occurs in the ternary alloy although only 2% Cu are present.

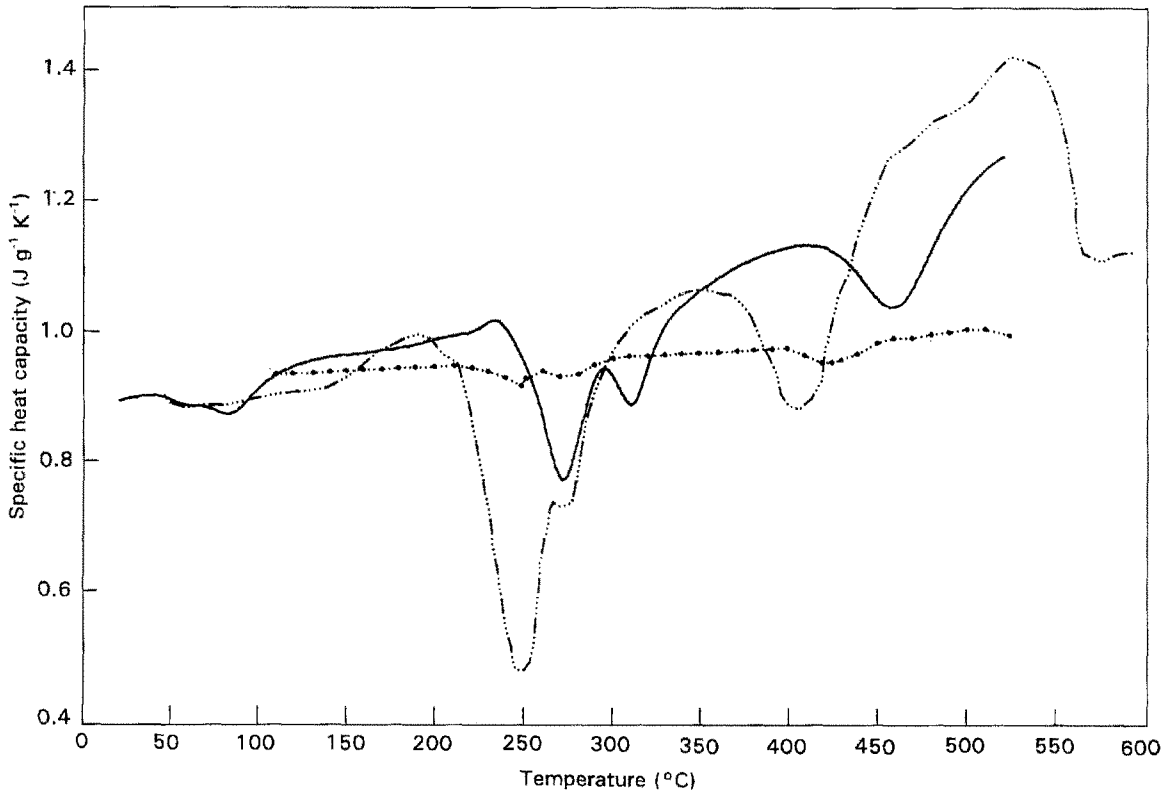

Figure 5 c_p-Evolution of ternary Al–Mg–Si alloys in as-quenched condition. ----●----, E0007000 [16] Al-0.62% Mg-0.37% Si 1 h/530 °C → 20 °C 2 K min^{-1}; –···–, E0007301 [17] Al-0.89% Mg-0.48% Si 2 h/560 °C → 0 °C 1–2 K min^{-1}; ——, E8000181 Al-2.0% Mg-1.1% Si 2 h/550 °C → 0 °C 20 K min^{-1}.

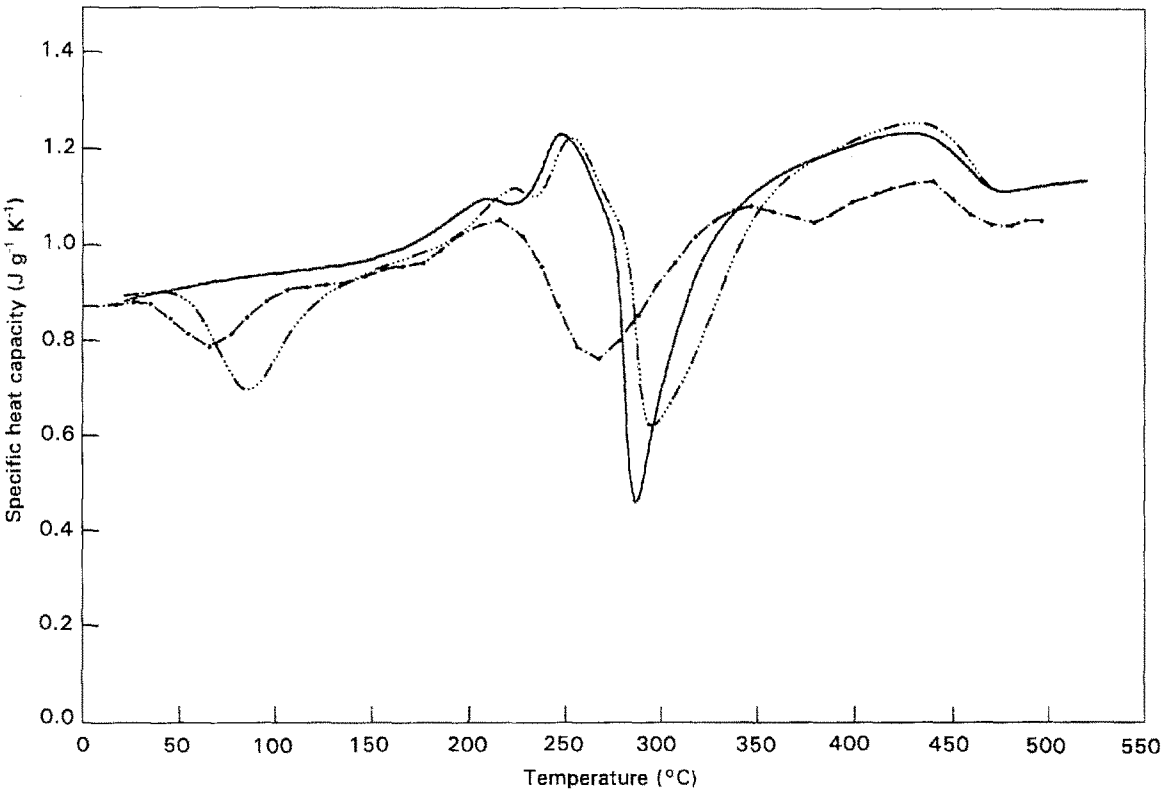

Figure 6 c_p-Evolution of ternary Al–Cu–Mg alloys. –·–·, E0006571 [18] Al-2.62% Cu-0.42% Mg 2 h/520 °C → 0 °C 2 K min^{-1}; ——···——, E8000059 Al-2.03% Cu-1.28% Mg 20 min/525 °C → 20 °C 20 K min^{-1}; ——, E8000061 Al-2.03% Cu-1.28% Mg 20 min/ 525 °C → 20 °C → 4 d/20 °C 20 K min^{-1}.

3.6. Ternary Al–Zn–Mg alloys

Fig. 7 demonstrates the influence of zinc concentration and solutionizing temperature on the c_p-evolution of solid solutions aged for one day at RT, maintaining the scan rate at 20 K min^{-1}. GP zone reversion is responsible for the first c_p-increase, and stable η ($MgZn_2$) dissolution for the very last one. With increasing homogenization temperature, more η is

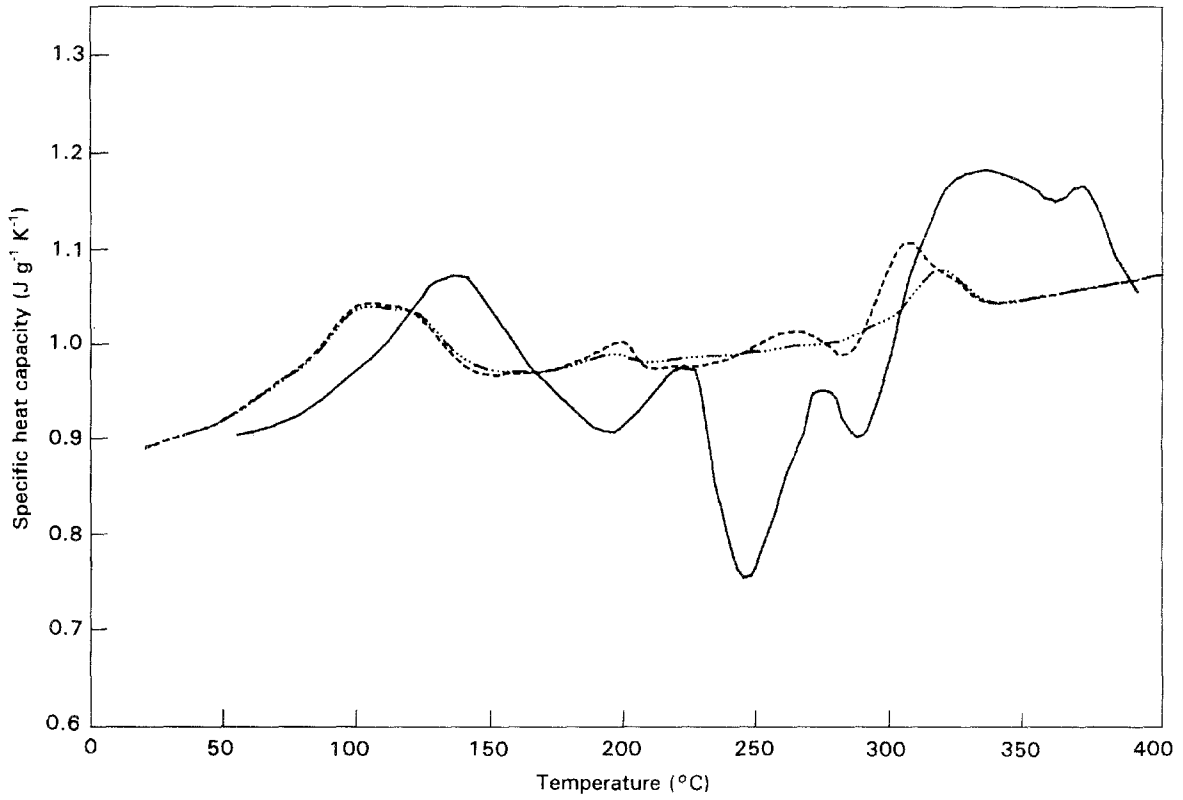

Figure 7 c_p-Evolution at 20 K min^{-1}, of ternary Al–Zn–Mg alloys. ——, E0006885 [23] Al-10.26% Zn-1.48% Mg 1 h/465 °C → 20 °C → 24 h/25 °C; —···—, E8000094 Al-4.99% Zn-1.10% Mg 2 h/400 °C → 0 °C → 24 h/20 °C; – – –, E8000099 Al-4.99% Zn-1.10% Mg 2 h/500 °C → 0 °C → 24 h/20 °C.

formed, as its nucleation during the analysis is aided by a higher density of vacancy-rich clusters [21]. In the intermediate temperature range, the c_p-variations of Al-5% Zn-1% Mg alloys are the more complicated the higher is the solutionizing temperature, and correspond to the formation of metastable phases, like η′, R, X, T′ [22] followed by their transformation and/or dissolution. The resultant effects overlap and may not be separated. Measurements at lower heating rates enable more substantial precipitation during the scan; the c_p-evolutions [21] finally have the same general shape as the curve shown in Fig. 7 for an alloy two times richer in zinc [23].

3.7. Alloys of series 2xxx

The influence of fabrication and heat treatment is exemplified in Fig. 8 for an alloy 2024 containing 4.4% Cu and 1.4% Mg besides 0.7% Mn, 0.2% Si, 0.2% Fe, 0.1% Zn, the sum of the other metallic elements being < 0.1%. As this composition is close to the one of alloy 2124 studied by Papazian [3], S′ and S formations predominate during heating, in agreement with Fig. 6.

For the alloy in the T4 ageing condition, S′ precipitation starts earlier in sheets cold-rolled to 1 mm than in 9 mm thick warm rolled plates as the former are more deformed, hence contain more dislocations which are nucleation sites for the S′-phase [20, 24]. The amount of S′ precipitated as deduced from a comparison of the enthalpy values is also higher than in Fig. 6, the Cu content of the alloy being greater.

Inasmuch as the extruded alloy is concerned, the c_p-values for the heat treatment T1 compare well with data obtained at a heating rate two times slower. The recommended values of Touloukian [25], however, do not take into account any precipitation and dissolution processes.

3.8. Alloys of series 5xxx

Four different alloys and heat treatments are compared; the respective chemical analysis (for concentrations > 0.1%) and material specifications are given below.

	5251 H24 1 mm sheet	5754 T1 extrusion	5086 O 1 mm sheet	5083 H24 1 mm sheet
Mg	1.97	2.94	3.94	4.49
Mn	0.25	0.23	0.35	0.69
Fe	0.28	0.18	0.31	0.29
Si	0.11	0.12	0.16	0.16

According to Fig. 9, the c_p-variations with respect to pure Al given in Fig. 3 are very small. The low temperature deviations observed in the two most Mg-rich alloys may be attributed to some GP zone reversion. At higher temperatures, the formation and dissolution of a more stable phase, probably Mg_5Al_8, occurs. As no GP zones appear in binary Al–Mg alloys containing < 4.5% Mg (see [26]), the action of impurity atoms, like Si, may be invoked. The data obtained at 10 K min^{-1} on extruded 5754 agree well.

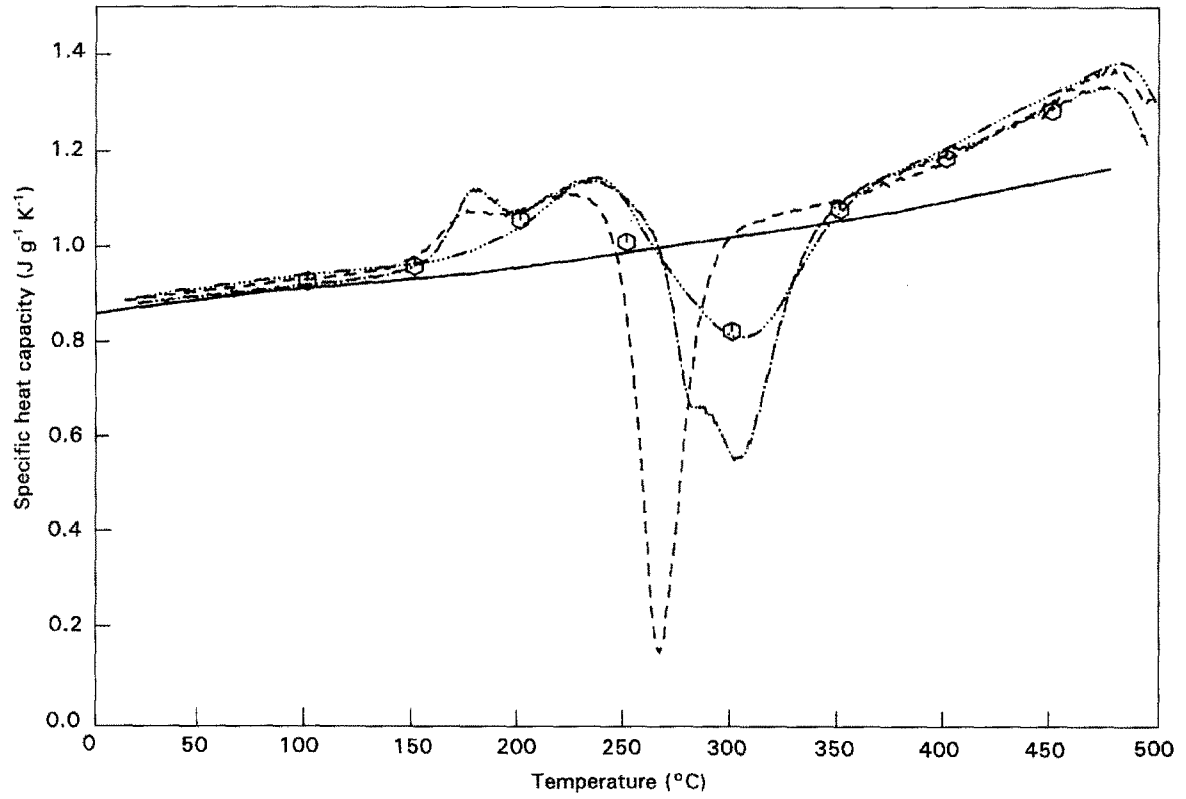

Figure 8 c_p-Evolution of 2024. ——, E0004738 [25]; – · · · –, E8000073 T1 extrusion 20 K min^{-1}; ⬡, E8000148 T1 extrusion 10 K min^{-1}; – – –, E8000188 T4 sheet 1 mm 20 K min^{-1}; – · – ·, E8000208 T4 sheet 9 mm 20 K min^{-1}.

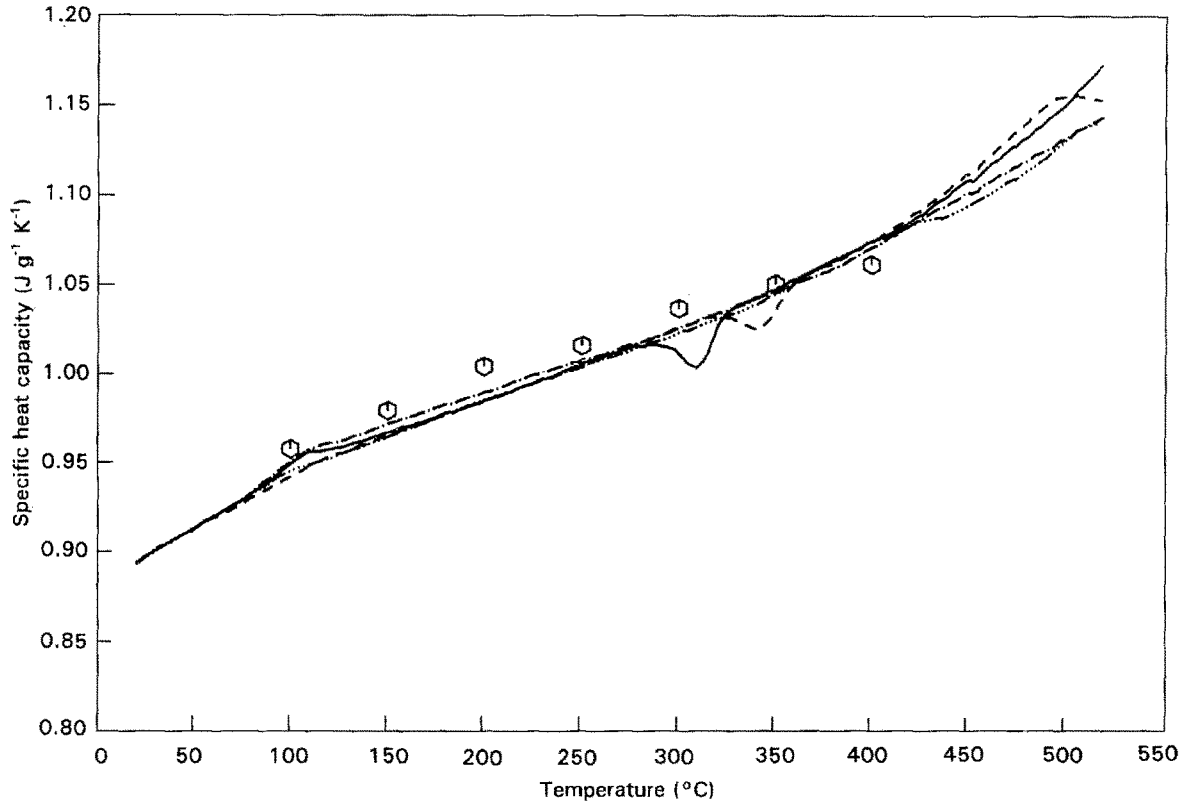

Figure 9 c_p-Evolution of alloys belonging to series 5xxx. ——, E8000201 5083 20 K min^{-1}; – · · · –, E8000063 5754 20 K min^{-1}; ⬡, E8000151 5754 10 K min^{-1}; – – –, E8000199 5251 20 K min^{-1}; – · – ·, E8000194 5086 20 K min^{-1}.

3.9. Alloys of series 6xxx

Fig. 10 shows the c_p-evolution of alloy 6082 containing mainly 0.93% Si, 0.75% Mg, 0.54% Mn and 0.28% Fe (mean values for extruded and rolled materials). Two different tempers, T5 for extrusions and T6 for sheets, are examined at 20 K min^{-1}; good agreement exists with data obtained at 10 K min^{-1} on temper T5. A comparison with Fig. 5 indicates that predominantly the β″-phase is present after these heat

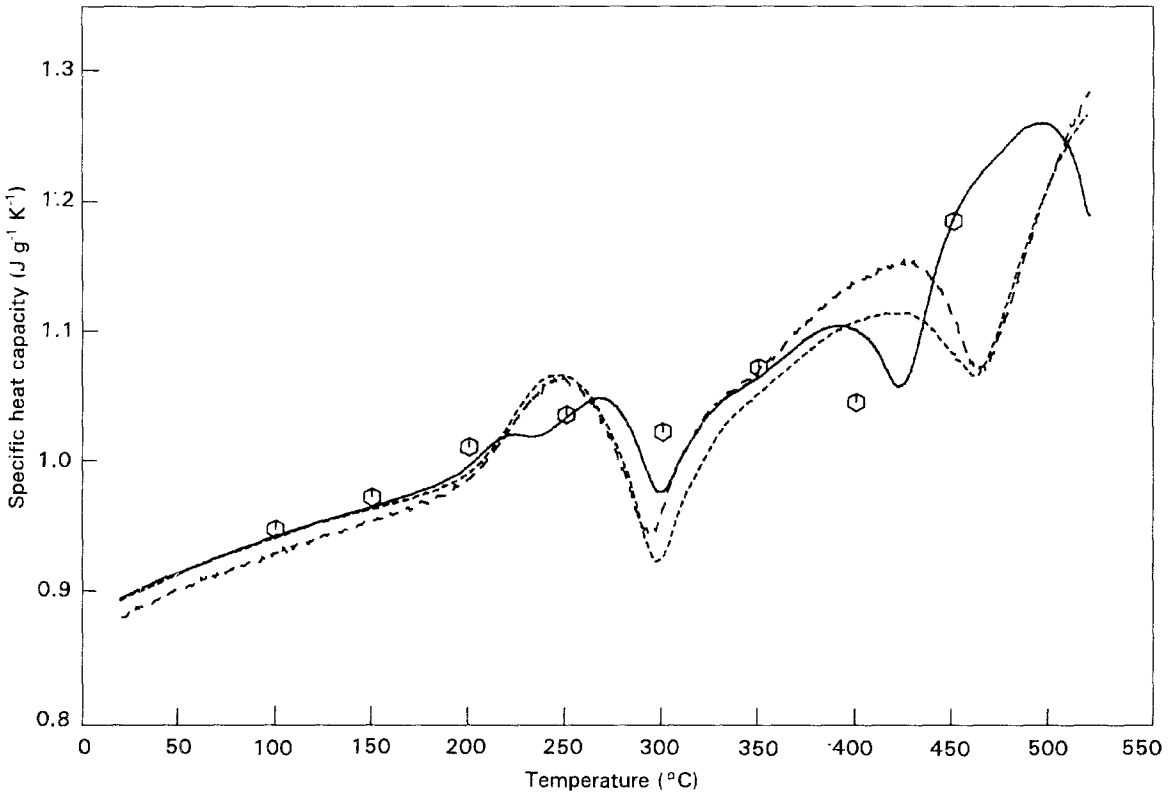

Figure 10 c_p-Evolution of 6082. ——, E8000067 T5 extrusion 20 K min^{-1}; ⬡, E8000093 T5 extrusion 10 K min^{-1}; - - - -, E8000189 T6 sheet 1 mm 20 K min^{-1}; – – –, E8000210 T6 sheet 9 mm 20 K min^{-1}.

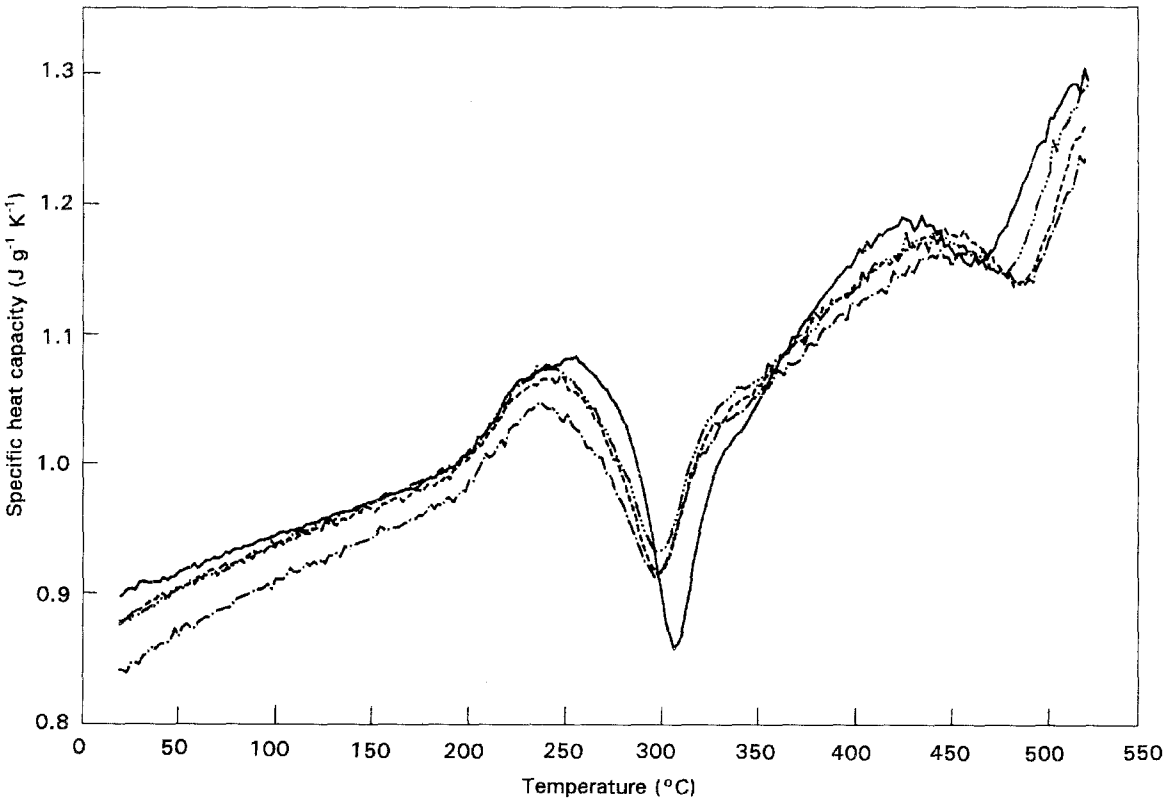

Figure 11 c_p-Evolution of 6061 in T6 temper and of MMCs based thereon (scanning rate 20 K min^{-1}). ——, E8000218 6061; ——···—, E8000219 6061 + 11.7 vol % Al_2O_3; - - - -, E8000220 6061 + 16.1 vol % Al_2O_3; – · –, E8000221 6061 + 20.5 vol % Al_2O_3.

treatments. After its dissolution during the DSC scan, the β′- and β-phases appear upon further heating. The c_p-curves for 1 (cold rolled) and 9 mm (warm rolled) thick sheets are not very different.

The influence of Al_2O_3 additions to an alloy 6061 in T6 condition is given in Fig. 11. The mean composition of the matrix alloys corresponds to 0.86% Mg, 0.64% Si, < 0.3% Cu, < 0.2% Fe, < 0.1% Cr.

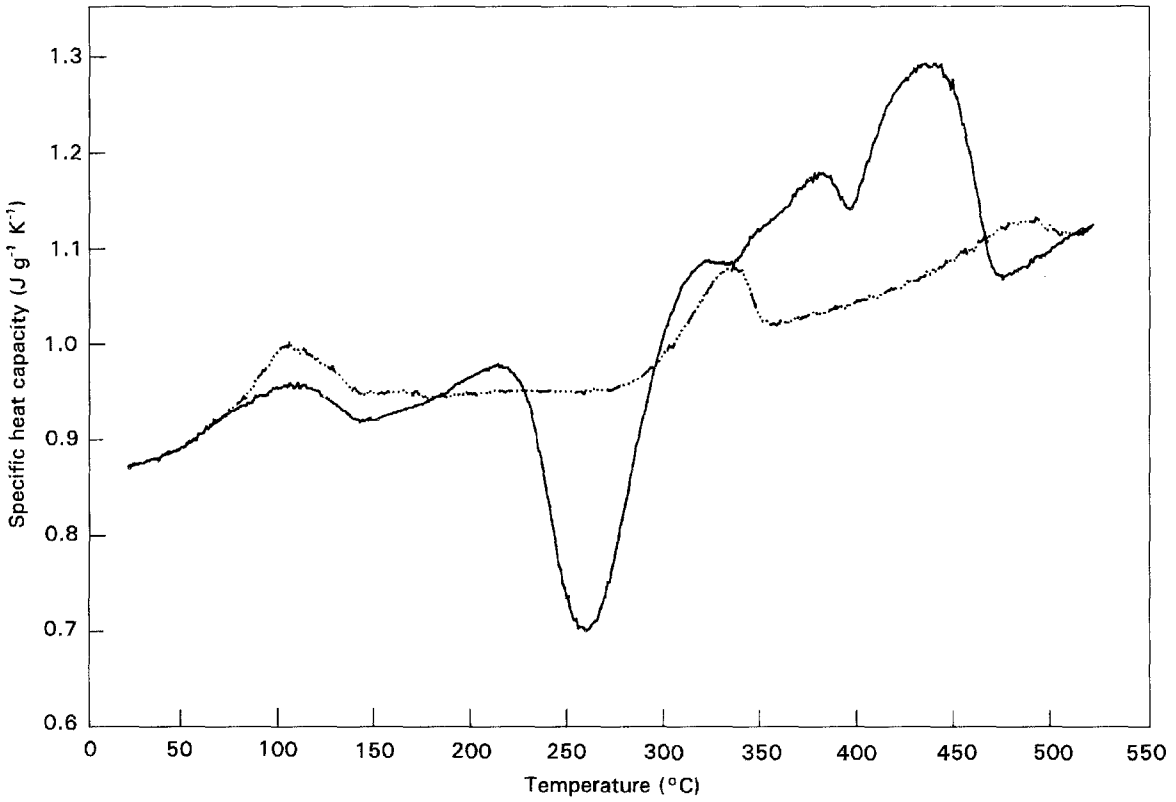

Figure 12 c_p-Evolution, at 20 K min^{-1}, of extruded alloys 7020 (–···–, E8000233) and 7075 (——, E8000234) after 2 h/400 °C → 0 °C → 24 h/20 °C.

Additions of Al_2O_3 decrease the c_p-values and lead apparently to initiation of β′ precipitation at a slightly lower temperature, but retard the β formation with respect to the matrix alloy.

According to Papazian [3], SiC additions to 6061 accelerate the precipitation of all metastable phases, in particular of β′, when heating as-quenched specimens. But less GP zones are formed and the alloy becomes quench sensitive.

It is in general observed that metal matrix composites having precipitation-hardenable matrices age faster than the unreinforced matrix alloy. Dutta and Bourell [27] propose that this is due to the dislocation density distribution effect on precipitation in MMCs which contain low volume fraction reinforcements. The same age-hardening processes operate, but the volume fractions of metastable phases are less. When preform binders are used in the fabrication of MMCs, they may degrade the age hardening response due to chemical interactions with the matrix [28].

Papazian [3] examined furthermore an alloy 6061 prepared by powder metallurgy. This process results in finer grain sizes and moderately accelerates β″ and β formation.

3.10. Alloys of series 7xxx

The chemical compositions of some alloys selected for this paper are given below along with the fabrication process.

	7020 extrusion	(7020) extrusion	7020 sheet	7075 extrusion
Zn	4.37	4.93	4.68	6.06
Mg	1.04	1.44	1.10	2.58
Cu	<	<	0.03	1.68
Mn	0.19	0.12	0.17	0.07
Cr	0.17	<	0.16	0.20
Fe	0.15	0.23	0.21	0.18
Si	0.10	0.10	0.11	0.11

Fig. 12 illustrates the influence of Cu in extrusions of alloys 7020 and 7075 aged for one day at 20 °C. Whereas the first alloy shows a c_p-evolution quite similar to that of the ternary alloy Al-5% Zn-1% Mg (curve E8000094 in Fig. 7), the Cu-rich alloy also displays features characteristic of the ternary Al–Cu–Mg alloys (Fig. 6) and attains the solid solution state at a much higher temperature than the Al–Zn–Mg alloys. The main constituent to precipitate in the alloy is the $MgZn_2$–CuMgAl phase [13].

The fabrication process does not modify sensibly the c_p-evolution of alloy 7020 available in the form of extrusions (condition T5) and sheets (T6 warm rolled to 9 mm and cold rolled to 1 mm). The curves in Fig. 13 agree with data derived at a two times slower heating rate. The stronger variations in the mean temperature range of alloy (7020) may be linked to its higher Zn and Mg contents leading to more η′ and η formation. As observed in the case of ternary AlZnMg alloys (Fig. 7), the main c_p-deviations come to an end around 350 °C, and the undulations at still

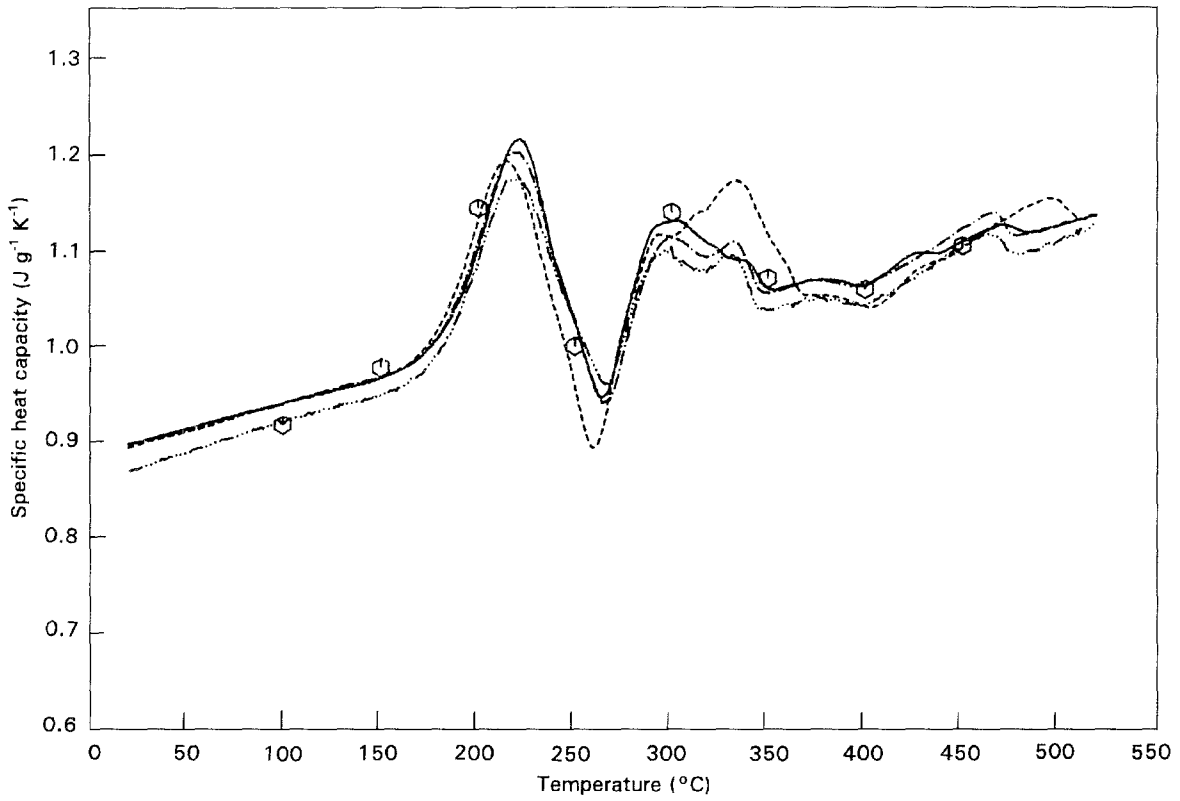

Figure 13 c_p-Evolution, at 20 K min^{-1}, of alloy 7020. ——, E8000069 7020 extrusion 20 K min^{-1}; ----, E8000083 (7020) extrusion 20 K min^{-1}; ⬡, E8000157 7020 extrusion 10 K min^{-1}; – · –, E8000190 7020 sheet 1 mm 20 K min^{-1}; – · · · –, E8000211 7020 sheet 9 mm 20 K min^{-1}.

higher temperatures may be attributed to impurity effects.

4. Conclusions

Several examples show which kind of information the c_p-values on pure and industrial Al alloys stored in the databank THERSYST are able to give. These alloys represent special cases inasmuch as one or even several metastable phases appear more or less slowly when a solution-treated alloy decomposes at lower temperatures. Quasi-equilibrium c_p-values are obtained only after long ageing times and are not very different from those of pure Al, if the sum of the additional elements does not exceed about 5%. This is also true in the presence of equilibrium phases at low volume fractions.

c_p-Measurements carried out by a dynamic method have the advantage of showing the evolution of the metastable and stable phases during continuous heating up to the solution treatment temperature. As the stability of each precipitate depends on its nature and size, the c_p-curve reflects the size distribution and relative amounts of the phases present before the analysis and indicates the precipitation and dissolution reactions which occur during further analysis, as a function of scan rate. Difficulties arise from the fact that reactions often overlap.

Once the reason for a c_p-discontinuity has been elucidated by phase identification with the help of transmission electron microscopy, the signature of the c_p-curves may be used for a rapid description of alloys in unknown metallurgical states. The influence of various parameters, like additional elements and reinforcements, fabrication process, thermomechanical treatment and scanning rate, on the precipitation and dissolution kinetics of the various phases and their relative amounts may be studied.

It is hoped that an atlas of c_p-curves may be set up which will contribute to the characterization of the different families of Al alloys and MMCs based thereon, in view of their selection and elaboration for specific applications.

Acknowledgements

The authors wish to thank Austria Metall AG for the fabrication of all industrial alloys studied as well as the French Ministère de la Recherche et de l'Espace, the German Bundesministerium für Forschung und Technologie and the Austrian Forschungsförderungsfonds für die gewerbliche Wirtschaft for financial support.

References

1. G. NEUER, R. BRANDT, G. JAROMA-WEILAND and G. PFLUGFELDER, *Int. J. Thermophys.* **10** (1989) 749.
2. S. C. MRAW, in "Specific Heat of Solids", edited by A. Cezairliyan (CINDAS Data Series, Vol. I-2. Purdue University West Lafayette USA. 1988) Chapter 11.
3. J. M. PAPAZIAN, *Metall. Trans.* **19A** (1988) 2945.
4. K.-I. HIRANO and H. IWASAKI, *Trans. Jpn Inst. Met.* **5** (1964) 162.
5. N. SWINDELLS and C. SYKES, *Proc. Roy. Soc.* **A168** (1938) 237.
6. A.-M. ZAHRA, C. Y. ZAHRA and M. LAFFITTE, *Scripta Metall.* **9** (1975) 879.

7. H.-H. JO and K.-I. HIRANO, *Mater. Sci. Forum* **13/14** (1987) 377.
8. A.-M. ZAHRA, M. LAFFITTE, P. VIGIER and M. WINTENBERGER, *Aluminium* **54** (1976) 357.
9. P. D. DESAI, *Int. J. Thermophys.* **8** (1987) 621.
10. A.-M. ZAHRA, C. Y. ZAHRA and J.-C. MATHIEU, *Z. Metallkde.* **71** (1980) 54.
11. H. P. DEGISCHER, C. Y. ZAHRA and A.-M. ZAHRA, *Z. Metallkde.* **73** (1982) 635.
12. A.-M. ZAHRA, C. Y. ZAHRA and R. CIACH, *J. Therm. Anal.* **26** (1983) 303.
13. L. F. MONDOLFO, "Aluminium Alloys: Structure and Properties" (Butterworth, 1979) p. 654.
14. M. Van ROOYEN and E. J. MITTEMEIJER, *Metall. Trans.* **20A** (1989) 1207.
15. E. OZAMURA and H. KIMURA, *Mater. Sci. Eng.* **8** (1971) 327.
16. T. HIRATA and S. MATSUO, *Trans. Jpn Inst. Met.* **12** (1971) 101.
17. T. MIYAUCHI, S. FUJIKAWA and K.-I. HIRANO, *Keikinzoku* **21** (1971) 565.
18. H. K. CHO and K.-I. HIRANO, ICTA-5, Kyoto (1977).
19. A.-M. ZAHRA, C. Y. ZAHRA, W. LACOM and K. SPIRADEK, in "Advanced Aluminium and Magnesium Alloys", edited by T. Khan and G. Effenberg (American Society for Metals, 1990) p. 633.
20. R. N. WILSON and P. G. PATRIDGE, *Acta Metall.* **13** (1965) 1321.
21. A.-M. ZAHRA, C. Y. ZAHRA, W. LACOM and H. P. DEGISCHER, *J. Mater. Sci.* **17** (1982) 3068.
22. H. P. DEGISCHER, W. LACOM, A.-M. ZAHRA and C. Y. ZAHRA, *Z. Metallkde.* **71** (1980) 231.
23. E. DONOSO, *Mater. Sci. Eng.* **74** (1985) 39.
24. A.-M. ZAHRA and C. Y. ZAHRA, *J. Therm. Anal.* **36** (1990) 1465.
25. "Thermophysical Properties of Selected Aerospace Materials. Part II: Thermophysical Properties of Seven Materials", edited by Y. S. Touloukian and C. Y. Ho (CINDAS, Purdue University, 1977).
26. M. Van ROOYEN, J. A. SINTE MAARTENSDIJK and E. J. MITTEMEIJER, *Metall. Trans.* **19A** (1988) 2433.
27. I. DUTTA and D. L. BOURELL, *Acta Metall. Mater.* **38** (1990) 2041.
28. C. FRIEND, R. YOUNG and I. HORSFALL, in "Developments in Science and Technology of Composite Materials", Eur. Conf. Compos. Mater., 3rd, edited by A. R. Bunsell, P. Lamicq and A. Massiah (Elsevier, 1989) p. 227.

Received 16 September 1993
and accepted 6 July 1994